



Radiolytic degradation of cellulosic materials in nuclear waste: Effect of oxygen and absorbed dose

Nele Bleyen^{a,*}, Veerle Van Gompel^a, Steven Smets^a, Samuel Eyley^b, Wim Verwimp^a, Wim Thielemans^b, Elie Valcke^a

^a Expert Group Waste & Disposal, SCK CEN, Boeretang 200, 2400, Mol, Belgium

^b Sustainable Materials Lab, Department of Chemical Engineering, KU Leuven, Campus Kortrijk, Etienne Sabbelaan 53, 8500, Kortrijk, Belgium

ARTICLE INFO

Handling Editor: Dr. Jay Laverne

Keywords:

Cellulose tissues
Gamma irradiation
Gas production
Polymerization degree
Reducing end groups
Crystallinity index

ABSTRACT

Lignocellulosic materials can be found in a significant fraction of the current low- and intermediate-level radioactive waste. During storage and disposal, radiolytic degradation of such materials can be expected, under oxic or anoxic conditions. This degradation may lead to a significant gas production and changes in the physico-chemical properties of the lignocellulosic materials, which can affect the formation of the known radionuclide-complexing agent isosaccharinic acid (ISA) as well as other (possibly complexing) degradation products during disposal. Hence, in the present work the radiolytic degradation of cellulosic tissues – realistically found in radioactive waste – was investigated under various storage and disposal conditions. For this, cellulosic tissues were exposed to γ -irradiation in gas-tight containers under oxic or anoxic conditions, at an absorbed dose ranging up to 1.4 MGy and at two different dose rates. Our results show that mainly H₂, CO and CO₂ are produced during irradiation of tissues, though also small amounts of CH₄ are formed. The presence of oxygen does not affect the generation of H₂, but results in a significant increase in the yields of CO, CO₂ and CH₄. Furthermore, radiation-induced chain scission is observed, causing a decreasing polymerization degree with increasing absorbed dose. Amorphization of the cellulose microstructure occurs significantly at high doses of gamma rays (≥ 0.8 MGy). An increase in the concentration of reducing functional groups is observed with increasing absorbed doses as well. For irradiation under anoxic conditions, this increase is correlated with the observed chain scission. In contrast, additional oxidation processes occur when irradiating cellulosic tissues in the presence of oxygen, resulting in a partially oxidized polymer backbone without causing considerably more chain scission or amorphization. These radiolytic changes to the cellulose structure, both under anoxic and oxic conditions, may enhance its hydrolytic degradation under the hyper-alkaline conditions of long-term final disposal, resulting in a faster production of radionuclide-complexing agents.

1. Introduction

Lignocellulosic materials are widely used in the nuclear industry, e.g. as paper, tissues, filters, wood and textiles. They make up a large quantity of certain, especially older, waste streams. In Belgium, cellulose-containing radioactive waste forms are proposed to be disposed of in either a surface facility (for low- or intermediate-level short-lived waste) or in a deep geological disposal facility (for intermediate-level long-lived waste). It is estimated for the near surface disposal facility that thousands of 400-L conditioned waste drums contain several kilograms of lignocellulosic materials per drum. For the geological disposal facility, a significant amount of 400-L drums will

even contain more than 10 kg of lignocellulosic materials per drum (Bleyen, 2020).

Cellulose is an unbranched linear homopolymer of $\beta(1,4)$ -linked D-glucopyranose monomeric units, with each unit being in the chair configuration (Ershov, 1998; Klemm et al., 1998). The number of incorporated glucose units per cellulose chain is referred to as the degree of polymerization or DP. Typical DPs of cellulose range from several hundred (for industrially processed cellulose) to over ten thousand for e.g. wood (Ioelovich, 2016; Updegraff, 1969). Cellulose chains have a non-reducing and a reducing end group. The reducing end group is a terminal monomeric unit with only one side involved in a glycosidic bond. Due to this, it consists of a cyclic hemiacetal in equilibrium with a

* Corresponding author.

E-mail address: nbleyen@sckcen.be (N. Bleyen).

<https://doi.org/10.1016/j.radphyschem.2023.111177>

Received 24 May 2023; Received in revised form 13 July 2023; Accepted 16 July 2023

Available online 20 July 2023

0969-806X/© 2023 The Authors. Published by Elsevier Ltd. This is an open access article under the CC BY license (<http://creativecommons.org/licenses/by/4.0/>).

reducing aldehyde group (Loelovich, 2016; Kontturi et al., 2006). During cellulose synthesis in nature, the cellulose chains are arranged in a well-defined supramolecular structure: many chains assemble using hydrogen bonds and Van der Waals interactions to form nanofibrils, which in turn aggregate to microfibrils. These microfibrils are usually embedded in a matrix consisting of hemicellulose and lignin. Hemicelluloses are a class of polysaccharides, composed of diverse sugar monomers, including xylose, arabinose, glucose, mannose and galactose. Unlike cellulose, hemicelluloses consist of shorter chains, which may be branched. They are rarely crystalline or fibrous in nature (Bajpai, 2018). Lignin is a group of highly aromatic and heterogeneous polymers. In general, lignins are amorphous and cross-linked, often containing a diverse set of functional groups, including aliphatics, phenolic hydroxyl and carbonyl groups (Moodley and Trois, 2021). Many cellulose microfibrils arranged in parallel comprise a macrofibril and several of these combine into cellulose fibers, with diameters ranging from 10 to 50 μm (Chinga-Carrasco, 2011; Gomez et al., 2008). The microfibrils contain distinct domains with variable levels of cellulose chain ordering, *i.e.* crystalline (highly ordered), paracrystalline (intermediately ordered) and dislocated (often referred to as 'amorphous') regions (Inagaki et al., 2010; Kulasinski et al., 2014; Martínez-Sanz et al., 2017; Moon et al., 2011; Nishiyama et al., 2003). The relative amount of highly ordered crystalline material within cellulose is represented as the crystallinity index (CI).

In radioactive waste, the cellulosic material is susceptible to two major degradation pathways. Firstly, due to the presence of radionuclides in the waste, radiolytic degradation of lignocellulosic materials will occur during storage and disposal, under either oxic or anoxic conditions. This degradation is known to lead to reactions of the polymer, such as chain scission (Arthur, 1971; Charlesby, 1955; Ershov, 1998), gas production (Arthur, 1958; Ershov, 1998) and the formation of carbonyl or carboxyl end groups (Ershov, 1998).

Secondly, due to the use of cement as immobilization matrix for the radioactive waste and as building material for the engineered barriers in the disposal facility, alkaline hydrolysis of cellulose will occur during disposal, resulting in the formation of soluble cellulose degradation products (Glaus et al., 2008; Van Loon and Glaus, 1997). Under the highly alkaline conditions prevailing in the disposal facility, some of these organic compounds, such as isosaccharinic acid (ISA), can form strong complexes with radionuclides present in the waste, which could reduce their sorption on cement phases and thus enhance their migration (Allard and Ekberg, 2006; Gaona et al., 2008; Vercammen et al., 1999). Several properties of cellulose may influence the hydrolytic degradation reactions and rates under alkaline conditions, *e.g.* morphological structure, crystallinity and degree of polymerization (Gentile et al., 1987; Haas et al., 1967; Mittal et al., 2011; Van Loon and Glaus, 1998). Changes made to these cellulose properties during radiolysis prior to hydrolytic degradation are thus expected to have an important effect on the overall production of radionuclide-complexing molecules in the waste.

A good knowledge of the radiolytic degradation of cellulosic materials in radioactive waste under storage and disposal conditions is therefore required, not only to assess the radiolytic gas production in the waste, but also to consider its effect on the (subsequent) hydrolytic degradation during disposal. Data on the radiolytic gas production by cellulose and lignocellulosic materials are however scarce, and strong discrepancies between the data exist. The radiolytic gas yields (G) for H_2 , CO and CO_2 production by γ -irradiation of pure cellulose range from 0.7×10^{-7} to 4.4×10^{-7} $\text{mol H}_2 \text{J}^{-1}$, from 0.9×10^{-7} to 3.3×10^{-7} mol CO J^{-1} , and from 1.0×10^{-7} to 6.0×10^{-7} $\text{mol CO}_2 \text{J}^{-1}$ (Arthur, 1971; Ershov, 1998; LaVerne et al., 2020). These wide ranges are most likely due to the many experimental differences, *e.g.* differences in the nature of the cellulose, and thereby its morphological and supramolecular structure, the absorbed dose applied (ranging from ~ 16 kGy to 0.6 MGy), the water content and/or the presence or absence of oxygen in the irradiation atmosphere. This latter variable in particular has not been

thoroughly investigated. Indeed, it is contradictory that some authors consider that an oxygen atmosphere during irradiation has no or no significant effect on the radiolytic yields, while on the other hand, oxygen consumption during irradiation has been observed (Arthur, 1971; Blouin and Arthur Jr, 1960; Ershov, 1998). Moreover, the yield factors were only determined either at high doses or at low doses, so no information on their evolution over a wide range of absorbed doses is available. Furthermore, due to an increased chemical complexity or the presence of aromatic groups, such as those in lignin (and in some types of hemicellulose), the radiolytic H_2 production by both compounds may be lower compared to cellulose, though again only few experimental results are available. Indeed, LaVerne et al. (2020) observed 1.2×10^{-7} and 0.3×10^{-7} mol J^{-1} as the G values for the production of H_2 by gamma irradiation (up to 0.06 MGy in air) of dry xylan (with aromatic side chains) and lignin, respectively. However, no data is available for the production of other radiolytic gases, nor for other hemicelluloses (without aromatic side chains). These knowledge gaps make it difficult to define a gas production rate from real cellulosic materials in radioactive waste.

Studies investigating the combination of physico-chemical changes of (ligno)cellulosic materials due to radiation are also scarce, especially for absorbed doses relevant for radioactive waste and under both oxic and anoxic conditions. Moreover, most of these studies were conducted on pure cellulose and not on real cellulose-containing materials that make up part of the organic radioactive waste. As these radiation-induced changes may affect the susceptibility of these materials to hydrolytic degradation, more detailed knowledge on their evolution during irradiation would allow for a better estimation of how these lignocellulosic materials would behave under disposal conditions.

The goal of this study was therefore to assess radiolytic degradation of cellulose-based materials expected to be present in radioactive waste under conditions during storage and final disposal. Both the radiolytic gas production and the evolution of the physical and chemical properties (DP, CI, morphology, release of water-soluble molecules and concentration of reducing end groups) of the tissues were assessed, including the effect of the absorbed dose (in a wide range of absorbed doses), the dose rate and the presence of oxygen during gamma-irradiation.

2. Materials and methods

2.1. Materials

Cellulosic tissues (Extra Soft Tork Facial Tissues, Belgium) were irradiated. All tissues were produced within the same batch (number 2211191/4), to avoid differences in the composition and cellulose properties between batches. The composition of the tissues was determined by PTS (Papiertechnische Stiftung; Germany), according to the standard procedures in Table 1. All procedures were applied to two subsamples.

2.2. Gamma-irradiation

Gamma-irradiation was performed at the Geuse II facility of SCK CEN (Belgium) (Fernandez et al., 2002). This facility consists of a large irradiation container surrounded by a maximum of 18 standard spent fuel assemblies from the BR2 reactor at SCK CEN. The samples are placed inside the facility on one of the two platforms of the inner rotating frame, which will ensure a homogeneous irradiation of each container. Given the emplacement of the spent fuel rods in relation to the position of the platforms, different dose rates are obtained at different vertical positions in the facility.

For this study, 15 to 100 g of tissues were irradiated inside stainless steel cylindrical containers (inner volume 1 L). Each container contained in- and outlet tubes (made of stainless steel) at the lids, which end in gas tight valves. These tubes allowed the connection of pressure sensors and gas sampling containers when the headspace needed to be sampled.

Table 1

Overview of the composition of the cellulosic tissues and the procedures used. The average content is derived from two measurements. The indicated uncertainty has been calculated using the Student's *t*-test for 95% confidence.

component	Average content (wt%)	Procedure
Dry content	95.6 ± 1.9	Using an infrared moisture analysis balance
α-cellulose	88.1 ± 0.6 ^a	Adapted from TAPPI standard T203cm-99 (TAPPI, 2009)
hemicellulose	11.4 ± 0.4 ^a	Based on alkaline solubility S ₅ (DIN standard 54356; (DIN, 1977))
lignin	0.5 ± 0 ^a	TAPPI standard T222 om-21 (TAPPI, 2021)
inorganic additives	0.54 ± 0 ^a	ISO standard 1762 (ISO, 2019)

^a Expressed in g per 100 g dry material.

After filling of the containers and welding of the lid to the container, leak tests were performed with He, to ensure that the system was gas tight. Subsequently, the head space of the container was replaced by pure argon (99.9997 vol% Ar, Air Products) or compressed air (Synthetic Air Zero Air 5.0, 20.7-21.1 vol% O₂, 78.9-79.3 vol% N₂, <1 × 10⁻⁴ vol% CO+CO₂, <2 × 10⁻⁵ vol% total hydrocarbons, <3 × 10⁻⁴ vol% H₂O) by extensive flushing, according to the test conditions in Table 2. For each atmospheric test condition, the headspace of three containers was sampled before irradiation to verify the lack of H₂, CO, CO₂, and CH₄ at the start of irradiation. All of them were below detection limit *i.e.* 2 × 10⁻³ vol% H₂, 10⁻³ vol% CO, 3 × 10⁻⁴ vol% CO₂, and 10⁻³ vol% CH₄. After sampling, the containers were refilled with Ar or compressed air. At the start of the irradiation, the pressure in all containers was 0.2 – 0.3 MPa (Table 2). An additional batch of tissues was irradiated in an open stainless steel container in which the tissues were in contact with the air in the irradiation facility (code C13). The irradiated tissues C13 were used to assess the effect of oxygen during irradiation on the radiolytic degradation, but not on the gas production.

Dose rates and absorbed doses were calculated based on the results of four dosimetries performed throughout the irradiation, *i.e.* at the start, after ~2.5 months, after 4 months, and at the end of the irradiation (after 5.5 months). This dosimetry was performed with Amber Perspex (PMMA, polymethylmethacrylate) dosimeters (type 3042, Harwell Dosimetries), according to the ISO/ASTM standard on the practice for dosimetry in radiation processing (ISO/ASTM, 2013). Based on the dosimetries, the evolution of the dose rate in the irradiation facility was determined and an exponential fit of the decay curve was derived. The total absorbed dose was then calculated for each vertical position based on the dose rate at the start of irradiation, the exponential decay of the dose rate, and the irradiation time. The total absorbed doses ranged from 10 kGy to 1.4 MGy (Table 2). For those tests irradiated with a total absorbed dose of 0.05 MGy and 0.8 MGy, the effect of the dose rate (0.3

Table 2

Gamma irradiation conditions. The uncertainty on the measured weight is 0.08 g and 4 kPa on the measured pressure (for 95% confidence). The uncertainties on the dose and dose rate are calculated as combined uncertainties, taking into account the uncertainty on the measured dose rates during the dosimetries and the uncertainty on the exponential fit of the decay curve.

Test code	Weight tissues (g)	Mean total absorbed dose (kGy)	Mean dose rate (kGy h ⁻¹)	Atmosphere during irradiation	Gas pressure at start (kPa)	Gas pressure at end (kPa)
Blank	100	0	0	/	/	/
C1	101.2	10 ± 2	0.63 ± 0.14	Ar	306	307
C2	100.2	47 ± 11	0.63 ± 0.14	Ar	304	309
C3	100.3	47 ± 11	0.63 ± 0.14	Air ^a	302	294
C4	101.2	48 ± 7	0.34 ± 0.05	Ar	301	305
C5	100.9	48 ± 7	0.34 ± 0.05	Air ^a	309	299
C6	101.2	180 ± 40	0.69 ± 0.16	Ar	301	318
C7	100.9	352 ± 56	0.67 ± 0.11	Ar	301	330
C8	100.9	760 ± 92	0.62 ± 0.08	Ar	205	264
C9	15.5	760 ± 92	0.62 ± 0.08	Air ^a	263	334
C10	100.0	764 ± 91	0.31 ± 0.04	Ar	205	263
C11	15.0	764 ± 91	0.31 ± 0.04	Air ^a	363	344
C12	40.4	1368 ± 160	0.55 ± 0.06	Ar	251	284
C13	100	172 ± 39	0.65 ± 0.15	Air ^b	^b	^b

^a Compressed air: 20.9 vol% O₂ and 79.1 vol% N₂.

^b Open container in contact with the air in the irradiation facility (at ~101 kPa pressure), containing ~21 vol% O₂, ~79 vol% N₂ and small amounts of other gases such as CO₂.

vs 0.6 kGy h⁻¹) and of the presence of O₂ during irradiation, was studied as well (Table 2). All irradiations were performed at room temperature.

2.3. Gas sampling and analysis

Before and after irradiation, the gas in the headspace of the containers was sampled by connecting a sampling container under vacuum. The concentrations of H₂, CO, CO₂ and CH₄ were assessed using a μGC-TCD (micro gas chromatography with thermal conductivity detector; μGC CP-4900, Varian). All gas samplings and analyses were performed at 22 ± 1.5 °C.

Radiolytic gas yield is defined as the concentration of gas formed as a function of the amount of energy deposited by ionizing radiation. It is denoted as *G* and expressed in mol J⁻¹. In general, the radiolytic yield is often not constant as a function of absorbed dose. A distinction is therefore made between the radiolytic yield at zero absorbed dose, *G*_{0,gas}, and the radiolytic yield at higher doses, *G*_{gas}. *G*_{0,gas} is determined as in Equation (1). *G*_{gas} is calculated similarly, but for higher doses.

$$G_{0,gas} = \frac{P \times \%_{vol} \times V_{free}}{RT \times D \times m} \quad \text{Equation 1}$$

where *P* is the total pressure (Pa) after irradiation, %_{vol} is the volume fraction of the gas after irradiation, *V*_{free}: free volume (m³) in the container, *D* is the absorbed dose (Gy) after irradiation (for *D* ≤ 100 kGy), *m* is the mass (kg) of the tissues, *R* is the ideal gas constant (*R* = 8.314 J mol⁻¹ K⁻¹), and *T* is the temperature (K).

2.4. Analysis techniques

After irradiation and gas analyses, the tissues remained in the closed stainless steel containers for at least 10 days, during which post-irradiation decay effects can occur (Bludovský et al., 1984; Kovalev

and Bugaenko, 2003).

All non-irradiated and irradiated tissues were cut into smaller pieces (few cm tall and wide) using clean scissors. For each test condition, the tissue pieces were mixed thoroughly, in order to avoid an impact of small differences in the absorbed dose applied to the tissues at different locations within the irradiation container. After mixing, subsamples were taken for the analyses described below. All samples were stored in the dark and under dry conditions until analysis.

2.4.1. Microscopic analyses

Scanning electron microscopy (SEM) analyses were performed on the non-irradiated and irradiated cellulose tissues. For this, the samples were mounted on a copper stub using carbon conducting tape. Samples were sputter-coated with gold (5 nm) in one cycle of 60s by a LuxorAu automated gold sputter coater (Luxor, Nazareth, Belgium). The coated samples were analyzed with a Phenom ProX tabletop SEM (Thermo Fisher Scientific Inc., Waltham, US), equipped with a backscatter electron detector at a working distance of 9 mm and 15 kV acceleration.

2.4.2. Molar mass distribution and polymerization degree

The molar mass distribution (MMD) was analyzed at Aalto University (Finland) by size-exclusion chromatography (Dionex Ultimate 3000 HPLC module, Thermo Fisher Scientific Inc., Waltham, US) equipped with four PLgel MIXED-A columns and multi-angle light-scattering (MALS) (Malvern Panalytical Ltd., Malvern, UK) and refractive index (RI, Showa Denko, Ogimachi, Japan) detectors, according to the procedure described by Pitkänen and Sixta (2020). Briefly, subsamples of (non-)irradiated tissues were dissolved in the eluent, i.e. 0.9% LiCl (Merck, Darmstadt, Germany) in HPLC grade N,N-dimethylacetamide (VWR Prolabo Chemicals, Radnor, US) via a solvent exchange procedure. In general, a tissue concentration of 1 mg mL⁻¹ was used, though for samples with a low molar mass, it was needed to increase the concentration up to 4 mg mL⁻¹ in order to improve the signal-to-noise ratio for light scattering. The injection volume was 100 µL.

Based on the obtained signals from the MALS and RI detectors, the M_n (number average molecular weight), M_w (weight average molecular weight), and the polydispersity (M_w/M_n) were determined. The average polymerization degree (DP_n or DP_w) can then be calculated as:

$$DP_n = \frac{M_n}{MW_{glucose}} \quad \text{with } M_n = \frac{\sum N_i M_i}{\sum N_i} \quad \text{Equation 2}$$

$$DP_w = \frac{M_w}{MW_{glucose}} \quad \text{with } M_w = \frac{\sum (N_i M_i^2)}{\sum N_i M_i} \quad \text{Equation 3}$$

where $MW_{glucose}$ is the molecular weight of anhydroglucose (162 g mol⁻¹), and N_i is the number of moles of a given cellulose fraction i having molar mass M_i (Hallac and Ragauskas, 2011).

Uncertainties on the molecular weights and DP s were calculated based on the standard deviation of 2 to 12 measurements per test condition and assuming a Student's t distribution.

All MMD data are available in the Mendeleev Data repository (<https://doi.org/10.17632/zs25y48cj5.1> Bleyen and Pitkänen, 2023).

2.4.3. Water-soluble fraction

To determine the water-soluble fraction, suspensions of tissues in water were prepared at a solid/liquid weight ratio 1/80 in glass vials. After 2 h, the solution was sampled and filtered using a pre-washed Acrodisc syringe filter with a PTFE membrane and a pore size of 0.45 µm (Merck, Belgium). Total dissolved organic carbon (DOC) concentrations were determined using a TOC/TIC analyzer with UV persulfate digestion (IL500 TC analyzer, Hach Lange, Belgium).

2.4.4. Reducing groups

A colorimetric biconchonic acid (BCA) assay was applied to determine the concentration of reducing (end) groups in the (irradiated)

tissues. In this assay, the Cu(II) in the reagent is reduced to Cu(I) by the reducing (end) groups in the tissues at alkaline pH (pH ~10). Subsequently, the reduced Cu(I) is complexed by BCA.

For this analysis, equal volumes of BCA reagent (prepared according to Garcia et al. (1993)) were added to tissue suspensions (0.6 to 10 mg mL⁻¹ dry tissue suspended in distilled water). The BCA method was adapted from Kongruang et al. (2004). After agitation, the mixtures were incubated at 75 °C for 30 min in a water bath. After 1 h of cooling to room temperature, the samples were agitated again and centrifuged for 2 min at 4180 g (centrifuge Z206A, Hermle, The Netherlands). The absorbance was measured at 560 nm using a UV-VIS spectrophotometer (Cary 500 Scan, Varian, France). Calibration was done using a glucose standard (1 mg mL⁻¹; Sigma Aldrich) diluted with distilled water at a range of concentrations. All samples were analyzed in (at least) triplicate. Uncertainties were calculated based on the standard deviation of 3 to 9 measurements per test condition and assuming a Student's t distribution.

The same method was performed on tissues (non-irradiated or irradiated at 0.8 MGy under Ar) previously washed in demineralized water (see Section 2.4.3) and dried in a fume hood at room temperature.

Note that the values obtained by BCA assay are presumably the total number of reducing groups per unit weight of cellulosic tissues, though under the conditions of the assay, i.e. at pH 10 and at a temperature of 75 °C. Measurements performed with other assays are performed under other test conditions (e.g. using 3,5-dinitrosalicylic acid (DNS) at pH 13 and 100 °C) and can therefore not be intercompared (Kongruang et al., 2004).

2.4.5. Crystallinity index

WAXS (Wide-angle X-ray scattering) characterization (performed at KU Leuven, Kulak Kortrijk Campus, Belgium) was carried out on the (non-)irradiated tissues to determine changes in the degree of crystallinity (or crystallinity index, CI) due to irradiation. The measurements were performed on a Xenocs Xeuss 2.0C laboratory beamline in transmission geometry, using a copper $K\alpha$ X-ray source (8.041 keV) with a point-collimated beam (1 mm diameter at the sample position). Scattered X-rays were detected using a Dectris Eiger 1M 2D hybrid photon-counting detector. The detector was moved through nine positions (three rows of three) perpendicular to the beam and the resulting images were stitched together to increase the accessible q -range (with q the scattering vector). The sample to detector distance (and therefore q vector) was calibrated using lanthanum hexaboride (NIST SRM660c). Data was collected with the entire beam path under vacuum (<0.1 kPa) during acquisition to reduce air scattering.

The resulting 2D detector images were azimuthally integrated to give 1D scattering curves. The intensity was corrected for transmission and converted to absolute intensity using a calculated linear absorption coefficient of 11.8 cm⁻¹. The background curve (empty beam) was subtracted from the sample curves prior to further processing.

The crystallinity index was calculated by Rietveld refinement (using TOPAS-academic v6) of two phases consisting of the cellulose I β phase published by Nishiyama et al. (2002) and an amorphous phase measured from amorphous cellulose generated by the dissolution of cellulose in phosphoric acid and precipitation in cold acetone. The phases were fitted to the data, allowing only small changes in unit cell parameters for the cellulose structure, one March-Dollase preferred orientation parameter in the [004] direction, and a flat background to account for possible errors in instrumental background subtraction. The fitting parameters were constrained to obtain a physically meaningful fit at the expense of a poorer mathematical fit to the data.

The crystallinity index was then determined using the Ruland method (Vonk, 1973) according to the following equation:

$$CI = \frac{\int_{q_0}^{q_1} I_c q^2 dq}{\int_{q_0}^{q_1} I_a q^2 dq} \quad \text{Equation 4}$$

where I_c is the intensity of the cellulose $I\beta$ scattering profile, I is the total calculated scattering intensity (sum of calculated crystalline and amorphous contributions), q is the scattering vector, given by $q = (4\pi \sin \theta) / \lambda$ and the integration limits q_0 and q_1 are 0.36 \AA^{-1} and 3.83 \AA^{-1} respectively.

Uncertainties were calculated based on the standard deviation of 3 to 5 measurements per test condition and assuming a Student's t distribution.

The datasets and patterns generated are available in the KU Leuven Research Data repository (<https://doi.org/10.48804/IPOIL9> (Eyley et al., 2023)).

3. Results

3.1. Radiolytic gas generation

Based on the total pressure measured in the gas-tight containers, the pressure increased during irradiation of tissues under anoxic conditions, while the inverse was observed under oxic conditions (Fig. S1, Supplementary Data). Under anoxic conditions, the pressure increased almost linearly with the absorbed dose. Only at the highest absorbed dose, a deviation from this linear relationship was observed. When the tissues

were irradiated in the presence of oxygen, the pressure decreased with an increasing absorbed dose. The observed pressure decrease is likely due to consumption of oxygen during radio-oxidation. At 0.8 MGy, the pressure (normalized to the mass of the tissues) had decreased by $\sim 1.5 \text{ kPa g}^{-1}$ on average.

The radiolytic gas production from cellulosic tissues was determined as a function of the absorbed dose, the dose rate and the atmosphere (anoxic vs oxic) during gamma irradiation. The gas yield factors for CO, CO₂ and H₂ are visualized in Fig. 1 and the exact values (for CO, CO₂, H₂ and CH₄) and statistical evaluation is given in Table S1 of the Supplementary Data. Table 3 shows the relative contribution of H₂, CO, CO₂ and CH₄ to the overall gas composition.

Mainly H₂, CO₂ and CO were formed during radiolysis of cellulosic tissues, though a small amount of CH₄ was also formed. Under anoxic irradiation conditions, H₂ was predominantly produced (in average 60% of the total gas), with a G_{0,H_2} value of $2.5 \pm 0.6 \times 10^{-7} \text{ mol J}^{-1}$. The G_{H_2} value remained stable in the lower dose range (up to 0.2 MGy). However, at higher absorbed doses, the G_{H_2} value decreased with increasing dose, *i.e.* the production of H₂ tends to level off gradually with increasing dose. A similar G_{H_2} value and its decrease with increasing absorbed dose was observed under oxic conditions. The presence of O₂ during irradiation did not affect the radiolytic H₂ production yield.

Under anoxic conditions, the CO and CO₂ production under gamma

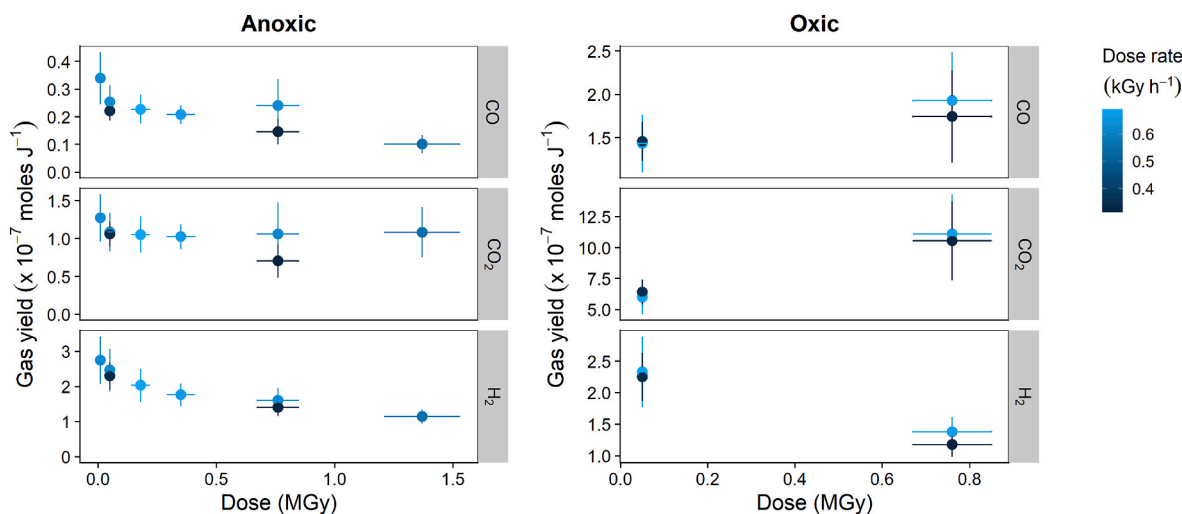


Fig. 1. Gas production yields for H₂, CO and CO₂ (as indicated on the right of each graph) during gamma irradiation of cellulosic tissues as a function of absorbed dose and applied dose rate (in kGy h⁻¹), under anoxic and oxic conditions. The error bars represent the uncertainty for a 95% confidence interval, calculated as a combined uncertainty on the pressure, gas concentration, weight of tissues and volumetric measurements.

Table 3

Relative gas concentrations (H₂, CO, CO₂ and CH₄) produced during gamma irradiation of cellulosic tissues as a function of the absorbed dose and the applied dose rate, under anoxic and oxic conditions. The relative amounts are calculated assuming that H₂, CO, CO₂ and CH₄ make up all gases. The indicated uncertainties represent the 95% confidence interval and take into account the uncertainties on the pressure and measured gas concentrations. The values with different superscript letters in a column are significantly different (according to a t -test, $\alpha = 0.05$).

Absorbed dose (kGy)	Dose rate (kGy h ⁻¹)	Atmosphere	% gas			
			H ₂	CO ₂	CO	CH ₄
10 ± 2	0.63 ± 0.14	Anoxic	63.0 ± 6.5 ^a	29.2 ± 2.9 ^a	7.8 ± 1.3 ^a	<DL
47 ± 11	0.63 ± 0.14	Anoxic	64.8 ± 6.3 ^a	28.5 ± 1.8 ^a	6.7 ± 0.5 ^{a,c}	<DL
47 ± 11	0.63 ± 0.14	Oxic	23.9 ± 1.8 ^b	61.2 ± 2.5 ^b	14.6 ± 0.6 ^b	0.33 ± 0.20 ^a
48 ± 7	0.34 ± 0.05	Anoxic	64.2 ± 5.9 ^a	29.6 ± 1.8 ^a	6.2 ± 0.4 ^c	<DL
48 ± 7	0.34 ± 0.05	Oxic	22.2 ± 1.8 ^b	63.1 ± 2.5 ^b	14.4 ± 0.6 ^b	0.28 ± 0.19 ^{a,b}
180 ± 40	0.69 ± 0.16	Anoxic	61.3 ± 4.6 ^a	31.7 ± 1.6 ^{a,c}	6.9 ± 0.3 ^a	0.22 ± 0.17 ^{a,b}
352 ± 56	0.67 ± 0.11	Anoxic	58.8 ± 6.1 ^{a,c}	34.2 ± 2.1 ^c	6.9 ± 0.4 ^a	0.13 ± 0.10 ^{a,b,c}
760 ± 92	0.62 ± 0.08	Anoxic	55.2 ± 14.8 ^{a,c}	36.4 ± 15.1 ^c	8.3 ± 3.4 ^{a,d}	0.10 ± 0.04 ^b
760 ± 92	0.62 ± 0.08	Oxic	9.6 ± 2.4 ^d	76.8 ± 25.5 ^b	13.3 ± 4.4 ^d	0.25 ± 0.08 ^a
764 ± 91	0.31 ± 0.04	Anoxic	62.2 ± 12.7 ^a	31.2 ± 10.0 ^{a,c}	6.5 ± 2.1 ^{a,c}	0.12 ± 0.05 ^b
764 ± 91	0.31 ± 0.04	Oxic	8.7 ± 2.3 ^d	78.2 ± 27.9 ^b	12.9 ± 4.6 ^d	0.18 ± 0.08 ^{a,b}
1368 ± 160	0.55 ± 0.06	Anoxic	49.1 ± 10.7 ^c	46.5 ± 15.0 ^c	4.4 ± 1.5 ^c	0.04 ± 0.03 ^c

< DL: below detection limit of the μ GC equipment (H₂: 2×10^{-3} vol%, CO₂: 3×10^{-4} vol%, CO: 1×10^{-3} vol%, CH₄: 1×10^{-3} vol%).

irradiation was lower compared to H₂, *i.e.* the G_{0,CO} and G_{0,CO2} values are $0.3 \pm 0.1 \times 10^{-7} \text{ mol J}^{-1}$ and $1.1 \pm 0.3 \times 10^{-7} \text{ mol J}^{-1}$, respectively. Under these conditions, the G_{CO2} value remained constant up to absorbed doses of $\sim 1.4 \text{ MGy}$, while the G_{CO} value decreased with increasing dose (statistical difference as from 0.05 MGy), similar to what has been observed for H₂. In contrast, under oxalic conditions, the G_{CO} and G_{CO2} values increased with absorbed dose, although for CO this increase is not statistically significant.

For all gases, the dose rate did not affect the G values, though the lower dose rate always resulted in a slightly (and statistically insignificant) lower G value, for all test conditions and absorbed doses.

Under anoxic conditions and at low absorbed doses ($\leq 200 \text{ kGy}$ for CO₂ and $\leq 800 \text{ kGy}$ for H₂ and CO), the relative concentrations of the gases remained stable in the atmosphere (Table 3): H₂ made up 61% (in average) of the gas atmosphere, while CO₂ and CO made up 30 and 7%, respectively (Table 3). These relative amounts are calculated assuming that H₂, CO, CO₂ and CH₄ are the only gases produced during radiolysis of cellulosic tissues. This is supported by the fact that the pressure increase observed during irradiation under anoxic conditions is equal to the sum of the partial pressures of the produced gases. At higher doses, relatively less H₂ and CO was produced, while the relative CO₂ content increased. This is linked to the fact that both G_{H2} and G_{CO} values decreased with absorbed dose, while the G_{CO2} remained constant over the entire dose range (Fig. 1). On the other hand, oxalic conditions during irradiation resulted in a significantly higher relative CO and CO₂ content, while the relative H₂ content decreased.

Additionally, for all test conditions, the relative CH₄ content in the atmosphere remained equal to or below 0.3%, though relatively more ($\sim 2.5\times$) CH₄ was produced under oxalic conditions compared to under anoxic conditions. The G_{0,CH4} value under anoxic conditions was too low to be determined and was $0.03 \pm 0.02 \times 10^{-7} \text{ mol J}^{-1}$ under oxalic conditions. At higher absorbed doses, the G_{CH4} value was derived for anoxic conditions, *i.e.* on average $0.005 \times 10^{-7} \text{ mol J}^{-1}$ (see Supplementary Data, Table S1).

Note that the observed gas pressure decrease during gamma irradiation at 0.8 MGy under oxalic conditions was rather extensive, given that the atmosphere only consisted of 21 vol% O₂. When taking into account the partial gas pressures of the produced gases, 70% to 90% of the initial O₂ content had been consumed after irradiation. This may imply that the O₂ content is a limiting factor for radio-oxidation and G_{CO} and G_{CO2} values at higher doses may be even higher when more O₂ would be available.

3.2. Irradiation-dependent evolution of physicochemical properties

3.2.1. Visual changes

When comparing the irradiated tissues to the non-irradiated ones, a clear yellow coloration was observed (Fig. S2 in Supplementary Data). The tissues had become darker and more brittle with absorbed dose. At 1.4 MGy, they seemed to have lost most of their mechanical strength.

However, SEM analyses of non-irradiated and irradiated tissues did not show major differences due to irradiation. Fig. S3 in the Supplementary Data compares the fiber structure of non-irradiated tissues and of tissues irradiated at 1.4 MGy under anoxic conditions. Although the latter contains more broken fibers than the non-irradiated tissues, the difference in the macrostructure is quite limited.

3.2.2. Molar mass distribution

Fig. 2 shows a clear shift in the MMD towards smaller sizes with an increasing absorbed dose. Differences in dose rate did not seem to affect the MMD. Furthermore, the MMD became more uniform, *i.e.* for absorbed doses above 50 kGy, the curves take on a more or less Gaussian distribution, indicating a random radiolytic degradation process. For the highest absorbed dose ($\sim 1.4 \text{ MGy}$), the cellulose chains became too small to be measured accurately with the SEC-MALS method.

A small (though consistent) impact of the atmospheric conditions during irradiation on the MMD can be observed, *i.e.* for all tissue samples irradiated under oxalic conditions (at 0.05 or 0.8 MGy), the relative abundance of the smallest chains is slightly higher and the MMD is less uniform after irradiation at 0.8 MGy compared to tissues irradiated under anoxic conditions (Figs. 2 and 3).

Due to the observed shift in the MMD, both M_n and M_w values clearly decreased with the absorbed dose (Fig. 4 and Table S3 in the Supplementary data). Significantly lower M_n and M_w values were obtained when the irradiation occurred under oxalic conditions compared to under anoxic conditions. For the tissues irradiated at the highest absorbed doses, less differences in M_n and M_w are noticeable. This can be attributed to the fact that chain scission of long chains results in a larger absolute decrease in M_n and M_w compared to chain scission of short chains. Furthermore, due to the limitations of the SEC-MALS method, the data for the tissues irradiated at 0.8 MGy and higher are more variable, providing a larger uncertainty on the M_n and M_w values.

Based on the weight-average molecular weight M_w obtained for the different tissue samples, the DP_w decreased from 1593 ± 101 (for non-irradiated tissues) to 58 ± 4 (tissues irradiated with $\sim 1.4 \text{ MGy}$ γ -rays). A similar evolution is observed for the number-average molecular weight M_n (Fig. S4), resulting in a DP_n of 454 ± 63 (for non-irradiated tissues) decreasing to 23 ± 10 (for tissues irradiated at $\sim 1.4 \text{ MGy}$). Plotting the reciprocal of the DP as a function of the

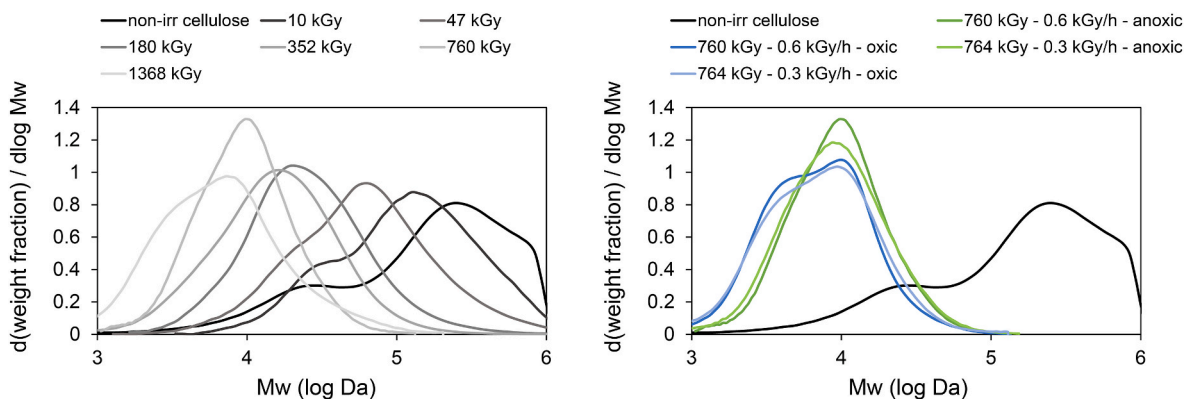


Fig. 2. Evolution of the molar mass distribution (MMD) of cellulosic tissues during gamma irradiation as a function of absorbed dose and applied dose rate (in kGy h⁻¹), under anoxic and oxalic conditions. Left: effect of absorbed dose on the MMD, for tissues irradiated under anoxic conditions and with the highest dose rate (on average 0.6 kGy h⁻¹). Right: effect of dose rate and irradiation atmosphere on the MMD.

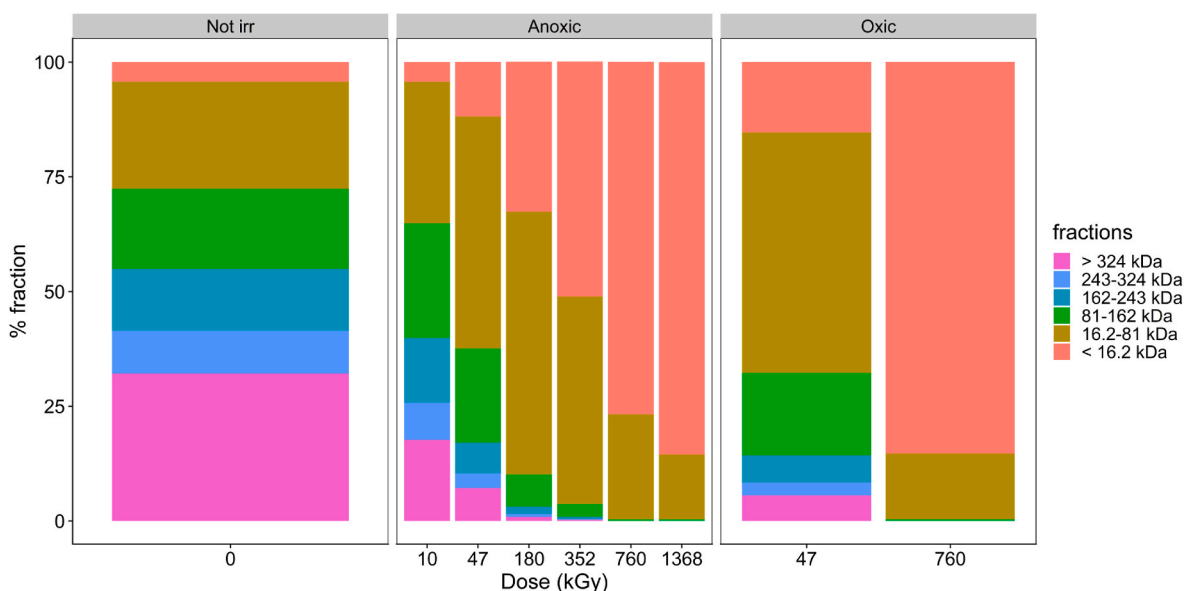


Fig. 3. Relative abundances of the different molecular weights (divided in fractions) during gamma irradiation of cellulosic tissues as a function of absorbed dose and irradiation atmosphere (anoxic vs oxic conditions). Only irradiations at ~ 0.6 kGy h^{-1} are shown. 'Not irr': non-irradiated tissues.

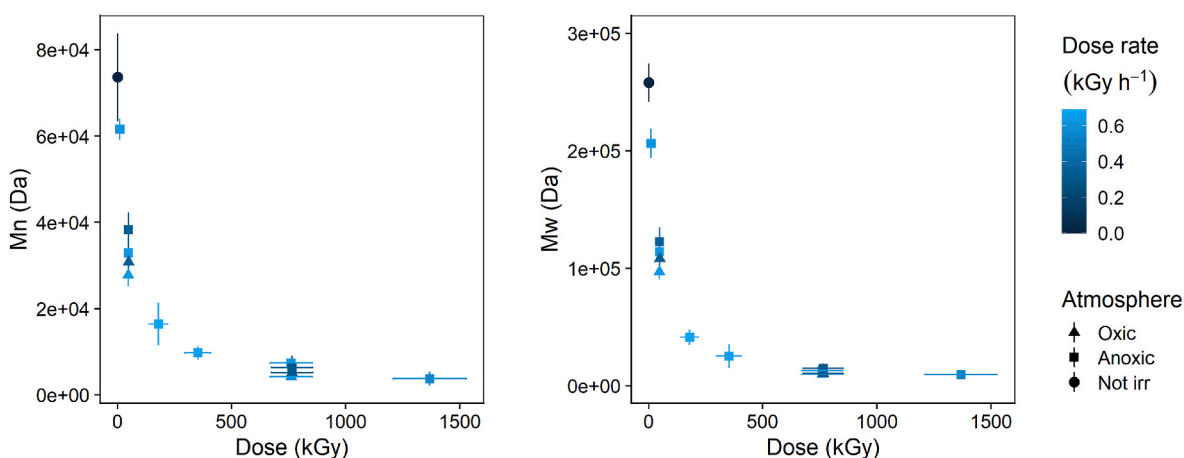


Fig. 4. Evolution of the number-average molecular weight (M_n) and weight-average molecular weight (M_w) of cellulosic tissues during gamma irradiation as a function of absorbed dose and applied dose rate (in kGy h^{-1}), under anoxic ('Ar') and oxic ('Air') conditions. 'Not irr': non-irradiated tissues. The error bars represent the uncertainty on the mean values based on the standard deviation and the t value ($n = 2-12$ and significance level $\alpha = 0.05$).

absorbed dose shows a linear dependency (Fig. S4). Note that higher regression coefficients are found for all linear regressions for tissues irradiated under oxic conditions compared to under anoxic conditions (Fig. S4). This is in line with the evolution of the MMD discussed above and in Fig. 2.

The polydispersity index of non-irradiated tissues is 3.7 ± 0.6 , indicating that the width of the MMD is large. The tissues therefore consist of a heterogeneous mixture of molecular sizes. During irradiation, this polydispersity index slowly decreased with increasing absorbed dose (Table S3 in the Supplementary Materials). As from an

Table 4

Estimated radiolytic scission yield G_s (based on equations (5) and (6)) observed during gamma irradiation of cellulosic tissues as a function of absorbed dose, applied dose rate, and irradiation atmosphere.

Absorbed dose (kGy)	Dose rate (kGy h^{-1})	Atmosphere	Radiolytic chain scission yield G_s ($\times 10^{-7}$ mol J^{-1})
47 ± 11	0.63 ± 0.14	Anoxic	3.6
47 ± 11	0.63 ± 0.14	Oxic	4.7
48 ± 7	0.34 ± 0.05	Anoxic	2.6
48 ± 7	0.34 ± 0.05	Oxic	4.0
760 ± 92	0.62 ± 0.08	Anoxic	1.6
760 ± 92	0.62 ± 0.08	Oxic	3.0
764 ± 91	0.31 ± 0.04	Anoxic	1.9
764 ± 91	0.31 ± 0.04	Oxic	2.4

absorbed dose of 0.2 MGy, it even slowly approached a value of 2, and thus less heterogeneity in molecular sizes.

The number of chain scissions (S) per polymer molecule can be estimated (based on Ershov (1998) and Henniges et al. (2012)) from the average M_w or M_n values (S_w and S_n respectively) and the applied absorbed doses:

$$S = \frac{DP_{w,0} - DP_w}{DP_w} = \frac{DP_{n,0} - DP_n}{DP_n} \quad \text{Equation 5}$$

The value for S_n can be used to calculate the chain scission yield (Henniges et al., 2012):

$$G_s = \frac{S_n}{M_{n,0} D} \quad \text{Equation 6}$$

Note that these equations are strictly only true for pure cellulose with a polydispersity of 2, *i.e.* for polymers with the most probable MMD and random chain scission. As our tissues are a mixture of hemicellulose and cellulose, and the polydispersity of the non-irradiated tissues is ~ 4 , Equation (5) can only be used as an estimation (Ershov, 1998; Henniges et al., 2012). Furthermore, crosslinking is not taken into account in this equation. This assumption seems valid, since crosslinking of cellulose during irradiation is assumed to be limited, compared to chain scission, at least at higher doses (see Section 4.1; Arthur, 1971; Ershov, 1998).

Figure S5 (Supplementary Data) and Table 4 give an overview of the estimated S and G_s values as a function of absorbed dose, applied dose rate and irradiation atmosphere. Based on this, an increase in S_n and S_w can be observed with increasing absorbed dose (Fig. S5 in the Supplementary Data). Furthermore, a higher value for G_s was obtained for tissues irradiated at lower absorbed doses compared to higher absorbed doses (Table 4), similar to what was observed for the H_2 production yields (see Section 3.1).

A trend towards a higher number of chain scissions is observed for irradiations under oxic conditions when compared to anoxic irradiations (Fig. S5 in the Supplementary Data). The yield factors also show a similar trend (Table 4), *i.e.* a higher radiolytic chain scission yield is obtained under oxic conditions compared to anoxic irradiations for all applied absorbed doses and dose rates. On the other hand, no clear effect of the dose rate on S or G_s can be observed.

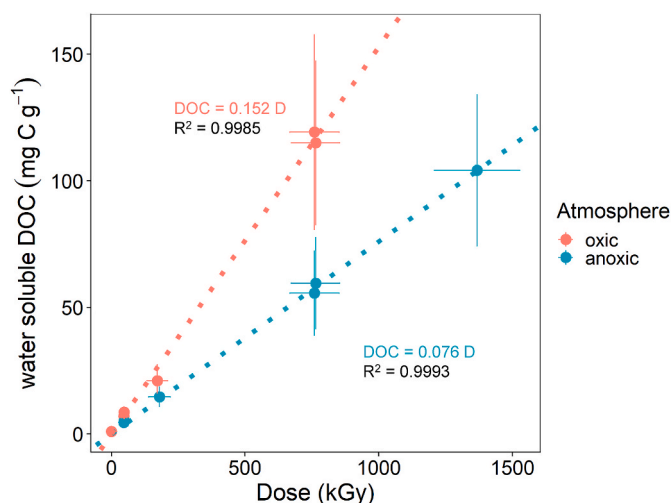


Fig. 5. Relationship between the absorbed dose and the water-soluble DOC fraction after gamma irradiation of cellulosic tissues, under oxic (red) and anoxic conditions (blue). As no impact of the dose rate was observed, no distinction based on dose rate was made. The error bars represent the combined uncertainty (with 95% confidence), taking into account the measurement uncertainty and the uncertainty on the measured weight of the tissues and water.

3.2.3. Water-soluble fraction

Fig. 5 shows the production of water-soluble organic compounds due to gamma irradiation. The values can be found in Table S5 in the Supplementary Data. A clear linear relationship can be observed between the released amount of water-soluble DOC and the absorbed dose, *i.e.* the water-soluble fraction of the tissues increases with increasing absorbed dose. Furthermore, irradiation under oxic conditions results in a higher water-soluble organic concentration compared to irradiation under anoxic conditions. The linear regression slopes indicate that the release rate of soluble DOC is about double for oxidically irradiated tissues compared to when they are irradiated under anoxic conditions.

Based on the amount of cellulose and hemicellulose in the tissues and under the assumption that hemicellulose consists of xylose monomers, the percentage of C in the tissues that is water-soluble can be estimated (Table S5 in the Supplementary Data). This shows that gamma-irradiation results in an increased weight fraction of water-soluble molecules in the tissues. This fraction also increases above the hemicellulose content (11.4 wt%) for tissues irradiated at high absorbed doses (≥ 0.8 MGy), suggesting that the increased weight fraction of water-soluble molecules due to irradiation is not due to radiolytic degradation of hemicellulose alone. This thus implies that either only cellulose or both cellulose and hemicellulose are degraded to water-soluble molecules during gamma-irradiation of cellulosic tissues.

3.2.4. Reducing groups

A clear increase in the concentration of reducing groups measured by BCA assay is observed with increasing absorbed dose and this for both irradiation atmospheres ('REGm'; Fig. 6). A linear regression provides a good prediction of the concentration of reducing groups (measured by BCA assay) as a function of the absorbed dose, for all test conditions. Significantly higher concentrations of reducing groups are obtained when the tissues were irradiated under oxic conditions compared to anoxic irradiation (Fig. 6 and Table S4 in the Supplementary Data). This difference is also observed in the four times higher regression coefficient for the linear regression between REGm and the absorbed dose under oxic conditions compared to anoxic conditions (Fig. 6). These results thus indicate that the presence of oxygen during irradiation results in an increased amount of oxidized functional groups.

When assuming that each cellulose and hemicellulose molecule has 1 reducing end group, the concentration of reducing end groups can be calculated based on the number-average molecular weight (Henniges et al., 2012).

$$REGt = \frac{1}{M_n} \quad \text{Equation 7}$$

with REGt as the theoretical concentration of reducing end groups (in mol g^{-1} tissue).

Similarly to REGm, a clear linear relationship between REGt and the absorbed dose is found, for all of the test conditions (Fig. 6; Table S4 in the Supplementary Data). The obtained regression coefficients for REGt as a function of the absorbed dose are quite similar for irradiations under both oxic and anoxic conditions, although a slightly higher value is obtained for irradiations under oxic conditions, linked to the MMD evolution under air (see Section 3.2.2). Both of these regression coefficients are also similar to the regression coefficient obtained for REGm under anoxic conditions.

When comparing the total concentration of reducing groups measured by BCA assay (REGm) and the calculated concentration of reducing end groups based on the M_n value (REGt), the position of the reducing groups within the polymer chains can be assessed. Indeed, as REGt is only indicative for the concentration of reducing end groups and REGm is the total concentration, the difference between both (REGad) can be used as an indicative value for the reducing groups on the polymer backbone (*i.e.* not positioned at the end of chain):

$$REGad = REGm - REGt \quad \text{Equation 8}$$

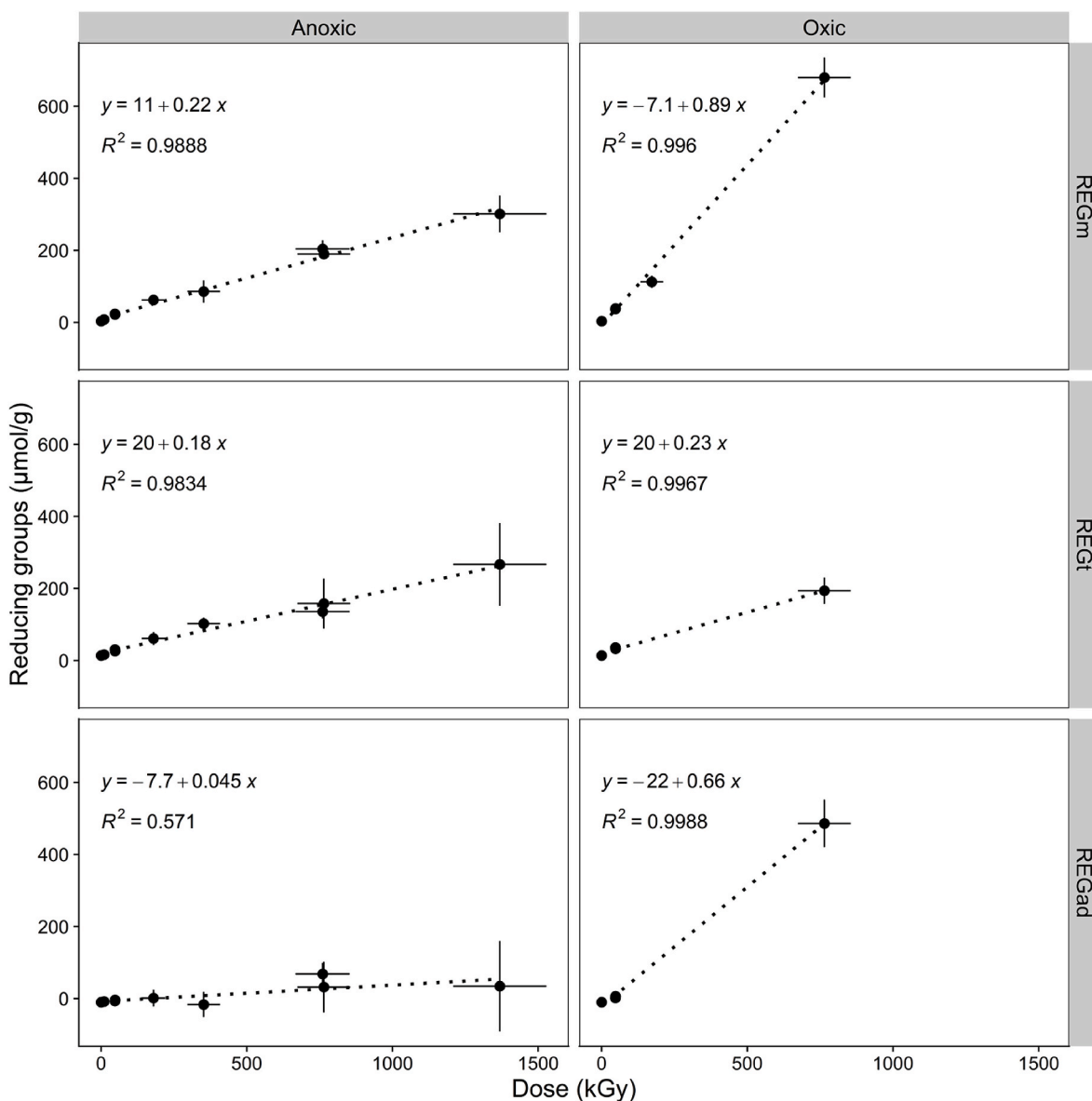


Fig. 6. Evolution of the concentration of reducing groups of cellulose tissues irradiated under anoxic conditions (left) and oxic conditions (right). REGm: concentration of reducing groups measured by BCA assay; REGt: theoretical concentration of reducing end groups calculated based on M_n by assuming that each polymer chain has 1 reducing end group; REGad: calculated difference between ‘total measured’ and ‘end groups based on M_n ’. For REGm and REGt, the error bars represent the uncertainty on the mean values based on the standard deviation and the t value ($n = 3-9$ and significance level $\alpha = 0.05$). The error bars of REGad represent the combined uncertainty (with 95% confidence), which takes into account the uncertainties on REGm and REGt.

For tissues irradiated under anoxic conditions, REGad remains close to zero (Fig. 6; Table S4 in the Supplementary Data), suggesting that the observed increase in REGm with increasing absorbed dose is predominantly linked to the formation of new reducing end groups caused by chain scission, rather than oxidation of the polymer backbone. In contrast, under oxic conditions, REGad increases significantly with the absorbed dose. In fact, the number of reducing groups along the backbone outnumbers the number of reducing end groups. These results imply that – besides chain scission – also a significant amount of radio-oxidation of the polymer backbone occurs during oxic irradiation of cellulosic tissues.

BCA analysis was also performed on seven (irradiated) tissues after washing the tissues with water and thus removal of the water-soluble organics (Fig. S6; Supplementary Data). Although mostly not statistically significant, a trend towards a decrease of the reducing group concentration (by 2 to 26%) was observed for all samples. This suggests that the reducing groups measured by BCA assay are predominantly found on the insoluble solid phase, although a limited amount of reducing molecules can be found in the water-soluble fraction as well.

3.2.5. Crystallinity index

WAXS analyses show a significant decrease of the crystallinity index of cellulose in the tissues during irradiation (Fig. 7; Table S6 in the Supplementary Data). A statistically significant reduction in crystallinity can be observed as from 0.8 MGy (with 95% confidence). This becomes even more apparent at higher doses. The decrease in crystallinity is likely already initiated at 0.4 MGy, but can only be confirmed statistically with lower confidence (90%).

Furthermore, neither the dose rate nor the presence of oxygen during irradiation affects the decrease in crystallinity, *i.e.* the crystallinity indices for all samples irradiated at either 0.05, 0.2 or 0.8 MGy, do not differ significantly (Fig. 7).

In all cases, the diffraction patterns demonstrate the presence of crystalline cellulose I β (see Supplementary Data in <https://doi.org/10.48804/IPOIL9> (Eyley et al., 2023)). A comparison between non-irradiated and irradiated tissues shows that gamma irradiation mainly results in a relative decrease in the intensity of the cellulose I β peaks and an increase in the intensity of the amorphous regions, while the diffraction pattern remains more or less constant.

4. Discussion

In general, radiation-induced degradation of cellulose is known to be initiated by a rapid production of long- and short-lived radicals. In this degradation mechanism, ionizing radiation first results in ionization of the cellulose, leading to an electron and a positively charged cellulose chain. Afterwards, charge migration along the chain is completed on defects in the crystal structure. After charge migration, recombination occurs and radicals are formed, preferentially at the weakest C₁-H and C₄-H bonds of the glucopyranose ring, though radicals could be formed on other C atoms as well. The hydrogen atoms formed will abstract hydrogen from other C atoms and H₂ is formed. However, the resulting long-chain radicals are unstable. Because of their strained structures, the radicalized cellulose chains quickly decompose, by scission of the glucopyranose ring and/or by cleavage of the O-glycosidic bond. The former process is believed to lead to the production of CO₂ and CO, while the latter results in the production of two cellulose chains, each with a non-reducing and a reducing end group (Arthur, 1971; Charlesby, 1955; Edimecheva et al., 2005; Ershov, 1998; Von Sonntag et al., 1976).

Although less studied, radiation-induced transformations of hemicellulose such as xylans are believed to be similar to cellulose and include chain scission at the glycosidic bond, degradation of the ring structures and the formation of reducing end groups, water-soluble sugars and gases such as H₂ and CO₂ (Ershov, 1998; Sánchez Orozco et al., 2012).

In the following sections, the induced physico-chemical changes to cellulosic tissues and the radiolytic gas production during gamma irradiation will be discussed, while keeping in mind the above-described degradation mechanism.

4.1. Radiation-induced chain scission and amorphization

The formation of radicals by gamma rays is assumed to be distributed along the entire polymer chains in the cellulosic tissues. As a result, longer chains are preferentially cleaved compared to shorter. Our SEC-MALS results seem to confirm this. At 10 kGy, mostly larger molecules appear to degrade, while the peak at ~30 kDa did not shift towards smaller molecules. At higher doses, the entire MMD shifted towards smaller molecules and the M_w and M_n values decreased with absorbed

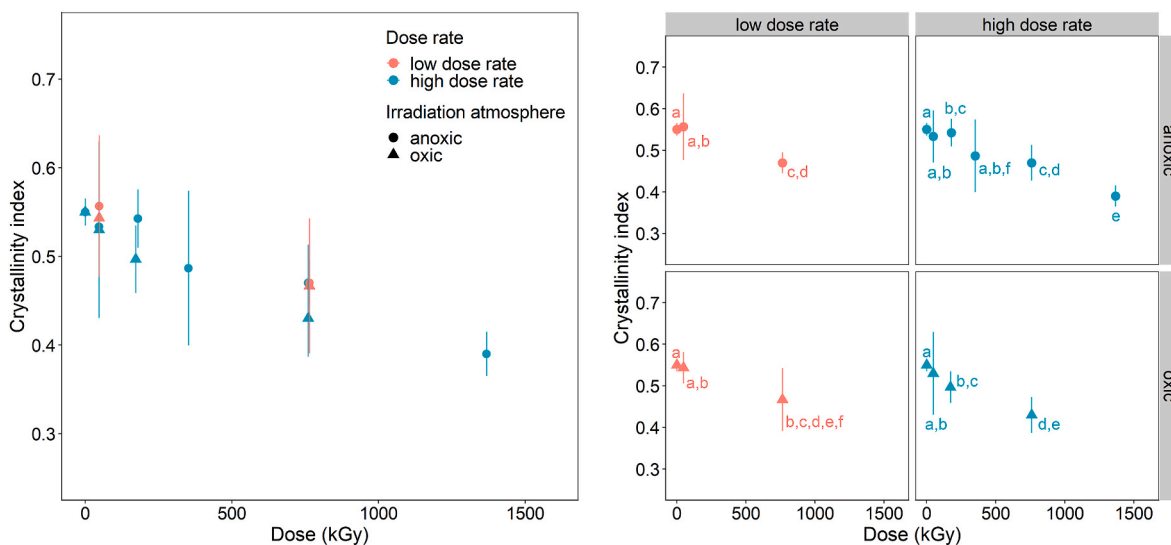


Fig. 7. Crystallinity index (CI) of cellulosic tissues after gamma irradiation, as a function of absorbed dose and applied dose rate (average ‘low’ dose rate 0.3 kGy h⁻¹, average ‘high’ dose rate 0.6 kGy h⁻¹) and irradiation atmosphere (anoxic or oxic conditions). The error bars represent the uncertainty on the mean values based on the standard deviation and the *t* value (*n* = 3-5 and α = 0.05). Left: all data; Right: data per dose rate and irradiation atmosphere, including an indication of the statistical differences between mean values according to a *t*-test (α = 0.05).

dose. The reciprocal of the correlated DP values increased linearly with the absorbed dose, and this for all tested dose rates and irradiation atmospheres and for absorbed doses up to 1.4 MGy. The regression coefficients of the inverse linear relationship found for irradiations of cellulosic tissues under anoxic conditions ($2.9\text{--}3.0 \times 10^{-5}$ for DP_n and $1.2\text{--}1.4 \times 10^{-5}$ for DP_w , Fig. S4) is quite similar to the values found for purified cotton or wood cellulose irradiated by gamma rays under vacuum (*i.e.* $4\text{--}7 \times 10^{-5}$ for DP_n and $2\text{--}5 \times 10^{-5}$ for DP_w ; absorbed doses up to 50 kGy (Kusama et al., 1976) or 100 to 150 kGy (Ershov, 1998)). Furthermore, increasing the absorbed dose resulted in more randomly distributed molecular masses, *i.e.* the MMD became more Gaussian and the polydispersity decreased towards 2 (*i.e.* most probable MMD) with increasing absorbed dose. This suggests that gamma irradiation of cellulosic tissues induces random chain scissions in polysaccharides.

The results of the WAXS analyses show a decrease in the crystallinity of cellulose with increasing absorbed dose, though only statistically significant as from 0.8 MGy (14% decrease in CI). Such amorphization of cellulose has been observed previously during irradiation with gamma rays, though the absorbed dose required to decrease the crystallinity is highly varying among studies: for pure cotton cellulose, absorbed doses above 1 MGy were required (Kovalev and Bugaenko, 2003), while the crystallinity of jute fibers decreased by 9% following a gamma absorbed dose of 100 kGy (Khan et al., 2006). Differences in the composition and the initial crystallinity of the lignocellulosic material may be responsible for the observed discrepancy in the threshold absorbed dose before observing a decrease in the crystallinity. At low absorbed doses, gamma irradiation did not affect the crystallinity of cellulose in the tissues. This can be explained by crosslinking in the amorphous regions (Kovalev and Bugaenko, 2003), which restricts the mobility of macrochain units. This crosslinking seems to become less important at higher absorbed doses, since the simultaneously occurring chain scissions causes the crosslinking to occur between shorter and more imperfect cellulose fragments (Kovalev and Bugaenko, 2003).

Based on our results, the impact of O_2 during gamma-irradiation on the molecular weight changes (and thus on the number of chain scissions) is very limited, though a trend towards smaller chains during irradiation under oxic conditions is observed based on the MMD and the estimated number of chain scissions. This is in agreement with results from Blouin and Arthur (1958), who only observed a limited decrease of the polymerization degree during gamma irradiation of purified cotton cellulose under either air or N_2 . Furthermore, no significant effect of O_2 on the radiolytic amorphization of cellulose in the tissues was observed. We can therefore assume that amorphization of the crystalline cellulose regions is mostly related to chain scission causing an increased mobility of macrochains, rather than to additional oxidation of the cellulose chain. The combination of the limited effect of O_2 on the radiolytically induced chain scission and the formation of crosslinks at lower absorbed doses, explains why oxygen does not affect the decrease of the crystallinity of cellulose during gamma irradiation.

No differences in MMD could be observed for the tissues irradiated at the same absorbed dose, though with different dose rates. Furthermore, no consistent effect of the dose rate on the crystallinity was observed either. Therefore, neither the depolymerization nor the amorphization seem to be affected by the dose rate, at least not in the range of dose rates tested in this study.

Note that SEM imaging of the tissue samples did not show major changes in the fiber morphology after irradiation, despite the observed depolymerization and amorphization at high absorbed doses. Only slightly more broken fibres can be observed in the tissues irradiated at 1.4 MGy compared to the non-irradiated tissues. SEM imaging therefore does not appear to be a suitable method to investigate radiolytic degradation of lignocellulosic materials.

4.2. Chemical alterations caused by irradiation

Our results clearly show an increase in the amount of reducing groups per g tissue with increasing absorbed dose, which is in line with previous research (Area and Ceradame, 2011; Arthur, 1971; Blouin and Arthur Jr, 1960; Bludovský et al., 1984; Dziędziela and Kotyńska, 1984; Sarosi et al., 2020) in which an increase in carbonyl, aldehyde and/or carboxyl groups was demonstrated after irradiation of cellulose or lignocellulosic materials. The enhanced yellow coloration and embrittlement of the tissues due to irradiation at increasing absorbed doses are also in agreement with the increased of reducing functional groups, either from cellulose itself or from hemicellulose. Indeed, it is known that carbonyl groups (both formed at the reducing end and in the backbone) are precursors for the formation of chromophores during ageing. Yellow coloration is therefore strongly correlated to the carbonyl content in cellulosic materials (Ahn et al., 2019).

When cellulosic tissues are irradiated under anoxic conditions, the measured concentration of reducing functional groups was highly similar to the calculated concentration of reducing end groups based on the M_n values. This suggests that the formation of reducing groups along the polysaccharide backbones (either cellulose or hemicellulose) is not significant under anoxic conditions. The radiolytic production of reducing groups in tissues under anoxic conditions is thus highly correlated to chain scission and the associated production of new chains with reducing end groups. On the other hand, a significant organic release was observed in water, which increased with increasing absorbed dose. About 25 wt% C in the tissues became water-soluble after irradiation at 1.4 MGy under anoxic conditions, indicating that thorough chain scission of smaller chains results in water-soluble molecules. This is in line with previous work on gamma-irradiated (up to 0.8 MGy) cotton cellulose, showing an increase in solubility in water (Arthur, 1971). Note that the results of a BCA assay performed on washed (anoxically irradiated) cellulosic tissues suggest that the reducing functional groups of the tissues are mostly situated on the insoluble solid phase. Nevertheless, a limited amount of soluble reducing molecules were produced during gamma irradiation of cellulosic tissues as well.

Irradiation of tissues under oxic conditions resulted in the formation of additional reducing functional groups, *i.e.* the concentration of reducing groups was ~50% higher after oxic irradiation at 0.05 MGy and even doubled at 0.8 MGy in comparison to the concentrations obtained after irradiation under anoxic conditions. A comparison of the measured concentration of reducing groups with the calculated concentration of reducing end groups (based on M_n), indicates that a significant amount of reducing groups is formed on the backbone of cellulose or hemicellulose in the tissues irradiated under oxic conditions. The observed difference in the formation of reducing groups for both irradiation atmospheres is in line with the observations by Arthur (1971), *i.e.* a difference in the Electron-Spin Resonance (ESR) spectra from cotton cellulose irradiated under oxygen versus nitrogen atmosphere was found. Arthur (1971) hypothesized that under an oxygen-rich environment, oxygen could react with a free radical to form for example a peroxy radical at one of the C atoms of the glucopyranose ring. Upon decomposition, a carbonyl or carboxyl group would then be formed on the polysaccharide chain, in some cases accompanied by chain scission. Such mechanism would indeed explain the observed increase in reducing functional groups and the slight shift of the MMD towards smaller molecules after irradiation of cellulosic tissues under oxic conditions. Furthermore, this additional radio-oxidation (using oxygen radicals) is in line with the observed pressure decrease (linked to oxygen consumption) in the containers initially filled with air.

Furthermore, tissues irradiated in the presence of oxygen have a higher water-soluble organic content compared to tissues irradiation under anoxic conditions. This is in contrast to the findings of Arthur (1971), who did not find considerable differences in solubility for cotton

cellulose gamma-irradiated up to 0.8 MGy under either an oxygen or a nitrogen atmosphere. Possibly, differences in the origin and the composition of the cellulosic material can explain this difference. Nevertheless, despite the higher water-soluble content, a BCA assay performed on washed (oxically irradiated) cellulosic tissues showed that the reducing groups are again mostly situated on the insoluble solid phase, similar to what was observed for anoxically irradiated tissues. Nevertheless, a similar decreasing trend was observed, which suggests that a limited amount of reducing, water-soluble organic molecules were formed during irradiation under oxic conditions as well. Based on previous research on gamma irradiation of cellulose or hemicellulose under oxygen-rich conditions (Arthur, 1971; Chen et al., 2016), at least part of these water-soluble compounds are expected to be sugars such as xylose, arabinose, glucose, but also small water-soluble oligosaccharides such as cellobiose and organic acids (e.g. glucuronic acid, gluconic acid) may have been formed. Given their reducing nature, this is in line with our results.

Note that although our findings demonstrate that a significant amount of oxidized (carbonyl or carboxyl) groups were introduced in the (hemi)cellulose backbone during oxidic irradiation, the crystallinity of the cellulose chains irradiated under different atmospheres did not differ. This would imply that the amount of oxidized groups in the backbone would be too small to change the hydrogen bond network in such a way that the crystallinity would be disturbed. Another possibility is that the formation of oxidized groups occurs preferentially in the amorphous regions of the cellulose chains or in the mostly amorphous hemicellulose. Such a preference may be explained by the limited accessibility of oxygen radicals inside the crystalline regions of the cellulose microfibrils.

4.3. Radiation-induced gas production

The results of the radiolytic gas production are in line with the general mechanism for radiolytic cellulose degradation as described above, i.e. H₂, CO and CO₂ were the most important gaseous degradation products after gamma irradiation of cellulosic tissues, although traces of CH₄ were found as well. Based on the obtained G values, the applied 2-fold difference in dose rate during gamma irradiation did not result in a significant difference in the G values for gas production. Either there is no dose rate effect, or it would only be detectable at larger dose rate differences.

The production of H₂ is originating from the abstraction of hydrogen from C atoms, which occurs independently from the presence or absence of reactive gases in the atmosphere. This explains why the presence of oxygen during irradiation does not affect the observed G_{H2} values for cellulosic tissues. The production yield of H₂ decreased with increasing dose, both under oxidic and anoxic conditions. Such a decrease in the yield of radiolytic degradation products with absorbed dose is common for the radiolysis of polymers and may be the result of intermediate and end products capturing the electrons, radicals and excitation energy, thereby retarding the further degradation of the polymer (Arthur, 1971; Ershov, 1998; Ponomarev and Ershov, 2014).

On the other hand, the radiolytic production of CO and CO₂ is affected by the presence or absence of O₂ during irradiation. Under anoxic conditions, the production of CO and CO₂ results only from cleavage of the glucopyranose ring of cellulose and likely also of the monomers in hemicellulose. This leads to G_{CO} and G_{CO2} values that are significantly lower than the G_{H2} values. The production yield of CO decreased with increasing dose, similar to H₂. The G_{CO2} value remained statistically constant with increasing absorbed dose, though a small trend towards a decrease can be observed for CO₂ as well.

When the tissues were irradiated under oxidic conditions, much higher concentrations of CO and CO₂ were produced compared to under anoxic conditions, showing the clear effect of oxygen radicals on radiolytic

cellulose degradation. Indeed, the G_{CO} and G_{CO2} values at ~50 kGy were five times higher under oxidic compared to under anoxic conditions. This difference becomes even larger at higher doses (at 0.8 MGy), when the G values increased tenfold.

Based on the enhanced radio-oxidation of the (hemi)cellulose chains (see Section 4.2) and the significantly higher G_{CO} and G_{CO2} values under oxidic conditions (compared to anoxic conditions), irradiation of cellulosic tissues in an oxygen-rich atmosphere not only results in chain scission and in the formation of carbonyl and carboxyl groups along the polymer backbone, but also in the production of additional CO and CO₂. The latter is likely not only linked to additional cleavage of the monomers, but also to further radiolytic degradation of the partially oxidized polymer backbone without causing considerable chain scission. In addition, further radiolytic degradation of smaller organic compounds in the presence of oxygen likely also contributed to the observed enhanced production of CO and CO₂, similar to what was proposed for the radiolytic degradation of aqueous sugar solutions under air (Ramírez-Cahero and Valdivia-López, 2018). Again, the additional radio-oxidation of the tissues by oxygen radicals is in agreement with the pressure decrease observed during irradiation under air.

In contrast to the decreasing radiolytic gas yields with absorbed dose observed under anoxic conditions, the radiolytic yield for CO₂ production increased with the absorbed dose under oxidic conditions. For CO, an increasing trend is observed under oxidic conditions as well, though this increase is not statistically significant. The increase in G_{CO2} (and G_{CO}) with absorbed dose can be explained by the fact that part of the CO and CO₂ is produced as a secondary degradation product, i.e. from further radiolytic degradation of radio-oxidized polysaccharide chains and/or smaller organic compounds. These secondary reactions become more dominant at higher absorbed doses.

Under anoxic conditions, the estimated value of G_S is twice as high as the sum of G_{CO} and G_{CO2}, while the inverse is observed under oxidic conditions with even a five-fold difference at higher absorbed doses. This shows that the chain scission process is the most dominant radiolytic degradation mechanism under anoxic conditions, while the production of CO and CO₂ by cleavage of the sugar monomers and decarbonylation and decarboxylation of radio-oxidized polysaccharides becomes more important under oxidic conditions. This is in line with the changes to the relative gas composition during irradiation under anoxic vs oxidic conditions, i.e. H₂ is the most important gas produced under anoxic conditions, while CO and especially CO₂ are predominantly produced under oxidic conditions.

Table S2 (Supplementary Data) compares the radiolytic yields for gas production from cellulosic tissues with the limited data available in literature. Note however that data over a wider range of absorbed doses was not available for cellulose, which makes comparison difficult, given the evolution of the G values with dose. The present study thus provides for the first time data on the G values for radiolytic H₂, CO, CO₂ and CH₄ production from cellulosic materials for a wide range of absorbed doses and under different irradiation conditions.

The comparison with literature data shows that the G_{H2} of cellulosic tissues is within the range obtained previously. The value is slightly lower than the value for pure cellulose samples obtained by LaVerne and coworkers, possibly due to the presence of hemicellulose, which has a lower G_{H2} value compared to cellulose (LaVerne et al., 2020) and tends to protect cellulose from radiolytic chain scission at low absorbed doses (Sarosi et al., 2020). The G_{CO} values are however rather low compared to the values observed in literature, for gamma-irradiation of cellulosic materials under both oxidic and anoxic conditions and at a similar absorbed dose. The G_{CO2} values obtained for cellulosic tissues, irradiated under anoxic conditions are similar to those found in literature (at a similar absorbed dose), while under oxidic conditions, the G_{CO2} values are higher than in literature. Note however that the G values found in literature are widespread and likely depending on the conditions during

irradiation (e.g. percentage of O₂ in the atmosphere or water content) and/or on the source (different commercial brands of cellulosic materials differ in content of carbonyl and carboxyl groups) and purity of cellulose.

Finally, to our knowledge, no data are available in literature for the value of G_{CH₄} for cellulosic materials. Although in our study only traces of CH₄ could be detected, it is still clear that methane is also formed during radiolytic degradation of cellulosic tissues and this to a higher extent under oxic conditions compared to anoxic conditions. Likely, the enhanced radio-oxidation and further degradation not only results the formation of CO and CO₂, but also some methane is formed.

5. Conclusions

As lignocellulosic materials make up a large quantity of certain nuclear waste streams, we can expect radiolytic degradation of such materials during storage and disposal, under either oxic or anoxic conditions. In this paper, both radiolytic gas production and the evolution of the physico-chemical properties (DP, CI, morphology and concentration of reducing end groups) of the tissues were assessed both under oxic and anoxic conditions and at a range of absorbed doses and dose rates. A combination between data on the gas production and on the physico-chemical changes provides sufficient data to build hypotheses on ongoing processes.

The results show that under an anoxic atmosphere, radiation-induced degradation of cellulosic tissues follows the general degradation mechanism, causing mostly production of H₂ and random chain scission. To a lesser extent, decomposition of the monomers of cellulose and hemicellulose occurs, thereby producing CO and CO₂. Finally, trace amounts of CH₄ are formed during irradiation as well, though with a much lower yield compared to H₂ (3 orders of magnitude lower). The chain scission is accompanied by a decrease in the polymerization degree and at higher doses (≥ 0.8 MGy) also in amorphization of the cellulose microstructure. Some crosslinking may occur, but seems only to be important at low doses. For each chain scission in (hemi)cellulose, two polymer chains are generated, predominantly each with a non-reducing and reducing end group, which thereby results in an overall increase in the reducing end group concentration. Formation of reducing groups along the polymer backbones does not occur significantly. Finally, additional chain scission of smaller chains results in an increasing degree of solubilization with an increasing absorbed dose.

When oxygen is present during irradiation, additional oxidation processes occur on top of the degradation processes that take place under anoxic conditions and that are unaffected by the presence of oxygen (e.g. chain scission, monomer ring cleavage and H₂ production). This results in a partially oxidized polymer backbone without causing considerably more chain scission or amorphization. In addition, more water-soluble organic molecules are formed compared to under anoxic conditions. Further radiolytic degradation of the partially oxidized polymer chain and/or smaller organic radiolytic degradation products results in a significant production of additional CO and CO₂. The secondary degradation processes could explain the increase in the G_{CO} and G_{CO₂} values with an increased absorbed dose. Under these conditions, cleavage of (partially oxidized) monomers in (hemi)cellulose and of smaller organic compounds becomes more important than radiolytic chain scission and CO₂ is the most dominant radiolytic gaseous end product. In addition, irradiation under oxic conditions also results in a 10-fold increase in the radiolytic yield of CH₄.

Under the anoxic and hyperalkaline conditions during final disposal of radioactive waste, hydrolysis of pre-irradiated cellulosic materials is expected to occur as well, resulting in the formation of soluble degradation products, such as ISA, which could enhance the transport of certain radionuclides towards the biosphere. As the production rate of ISA is believed to increase with increasing reducing end group concentration and crystallinity (Van Loon and Glaus, 1998; Van Loon et al., 1999), the radiolytic degradation of these materials prior to hydrolysis

may affect the ISA production rate. This will be investigated further in the future.

CRediT author statement

Bleyen Nele: Conceptualization, Methodology, Validation, Formal analysis, Investigation, Data curation, Writing – Original draft, Visualization, Project administration; Van Gompel Veerle: Methodology, Validation, Investigation; Smets Steven: Methodology, Validation, Investigation; Eyley Samuel: Methodology, Validation, Investigation, Formal analysis, Investigation, Data curation, Writing – Original draft, Writing – Review & Editing, Visualization; Verwimp Wim: Investigation; Thielemans Wim: Resources, Writing – Review & Editing, Supervision, Project administration, Funding acquisition; Valcke Elie: Conceptualization, Resources, Writing – Review & Editing, Supervision, Funding acquisition.

Funding

The project leading to this paper has received funding from the European Union's Horizon 2020 research and innovation programme under grant agreement No 847593 and has been co-funded by ONDRAF/NIRAS as part of the broader framework of a public-public partnership between ONDRAF/NIRAS and SCK CEN. Wim Thielemans and Samuel Eyley further acknowledge financial support from KULEuven (grants IBOF/21/105 and C3/20/120), and Research Foundation Flanders (grants GOA1219N and G082121N).

Declaration of competing interest

The authors declare that they have no known competing financial interests or personal relationships that could have appeared to influence the work reported in this paper.

Data availability

I have shared the link to my data in the Manuscript, available after publication

Acknowledgements

Supporting work performed by Katrien Hendrix (SEM analyses, SCK CEN, Belgium), Leena Pitkänen and Timo Ylönen (SEC-MALS, Aalto University, Finland), Göran Verpoucke and Prisca Verheyen (DOC analyses, SCK CEN, Belgium) is highly appreciated. Finally, we thank Delphine Durce (SCK CEN, Belgium), Benny de Blochouse (ONDRAF/NIRAS, Belgium), and all colleagues within the EURAD project WP CORI for their constructive comments and suggestions to this study.

Appendix A. Supplementary data

Supplementary data to this article can be found online at <https://doi.org/10.1016/j.radphyschem.2023.111177>.

References

- Ahn, K., Zaccaron, S., Zwirchmayr, N.S., Hettegger, H., Hofinger, A., Bacher, M., Henniges, U., Hosoya, T., Potthast, A., Rosenau, T., 2019. Yellowing and brightness reversion of celluloses: CO or COOH, who is the culprit? *Cellulose* 26, 429–444. <https://doi.org/10.1007/s10570-018-2200-x>.
- Allard, S., Ekberg, C., 2006. Complexing properties of alpha-isosaccharinate: stability constants, enthalpies and entropies of Th-complexation with uncertainty analysis. *J. Solut. Chem.* 35, 1173–1186. <https://doi.org/10.1007/s10953-006-9048-7>.
- Area, M.C., Ceradame, H., 2011. Paper aging and degradation: recent findings and research methods. *Bioresources* 6, 5307–5337. <https://doi.org/10.15376/biores.6.4.5307-5337>.
- Arthur, J.C., 1958. Part II: proposed mechanism of the effects of high energy gamma radiation on some of the molecular properties of purified cotton. *Textil. Res. J.* 28, 204–206. <https://doi.org/10.1177/004051755802800303>.

- Arthur, J.C., 1971. Reactions induced by high energy radiation. In: Bikales, N.M., Segal, L. (Eds.), *Cellulose and Cellulose Derivatives*. Wiley Interscience, pp. 937–975.
- Bajpai, P., 2018. Wood and fiber fundamentals. In: Bajpai, P. (Ed.), *Biermann's Handbook of Pulp and Paper*. Elsevier Place, pp. 13–54.
- Bleyen, N., 2020. Degradation of Cellulose under Disposal Conditions. State-Of-The-Art Report. External Report SCK CEN-ER-0791. SCK CEN, Mol, Belgium.
- Bleyen, N., Pitkänen, L., 2023. SEC-MALS data irradiated cellulosic tissues. Mendeley Data. <https://doi.org/10.17632/zs25y48cj5.1>.
- Blouin, F.A., Arthur, J.C., 1958. The effects of gamma radiation on cotton - Part I: some of the properties of purified cotton irradiated in oxygen and nitrogen atmospheres. *Textil. Res. J.* 28, 198–204. <https://doi.org/10.1177/0040517558028003>.
- Blouin, F.A., Arthur Jr., J.C., 1960. Degradation of cotton in an oxygen atmosphere by gamma radiation. *J. Chem. Eng. Data* 5, 470–475. <https://doi.org/10.1021/j60008a016>.
- Bludovský, R., Procházková, M., Kopoldová, J., 1984. The influence of oxygen on the radiolytic products of cellulose. *J. Radioanal. Nucl. Chem.* 87, 69–79. <https://doi.org/10.1007/BF02167672>.
- Charlesby, J.A., 1955. The degradation of cellulose by ionizing radiation. *J. Polym. Sci.* 15, 263–270. <https://doi.org/10.1002/pol.1955.120157921>.
- Chen, J., Wang, L., Su, X., Wang, K., Wu, X., Chen, L., Xiong, X., Zhou, H., Liu, Y., 2016. Structure, morphology, thermostability and irradiation-mediated degradation fractions of hemicellulose treated with γ -irradiation. *Waste Biomass Valor* 7, 1415–1425. <https://doi.org/10.1007/s12649-016-9489-1>.
- Chinga-Carrasco, G., 2011. Cellulose fibres, nanofibrils and microfibrils: the morphological sequence of MFC components from a plant physiology and fibre technology point of view. *Nanoscale Res. Lett.* 6, 417. <https://doi.org/10.1186/1556-276X-6-417>.
- DIN, 1977. Testing of Pulp - Determination of the Alkali Solubility of Pulp. DIN standard 54356.
- Dziedzic, W.M., Kotyńska, D.J., 1984. Functional groups in γ -irradiated cellulose. *Radiat. Phys. Chem.* 23, 723–725. [https://doi.org/10.1016/0146-5724\(84\)90030-X](https://doi.org/10.1016/0146-5724(84)90030-X).
- Edimecheva, I.P., Kisel, R.M., Shadyro, O.I., Kazem, K., Murase, H., Kagiya, T., 2005. Homolytic cleavage of the O-glycoside bond in carbohydrates: a steady-state radiolysis study. *J. Radiat. Res.* 46, 319–324. <https://doi.org/10.1269/jrr.46.319>.
- Ershov, B.G., 1998. Radiation-chemical destruction of cellulose and other polysaccharides. *Russ. Chem. Rev.* 67, 353–375. <https://doi.org/10.1070/RC1998v067n04ABEH000379>.
- Eyley, S., Bleyen, N., Thielemans, W., 2023. X-Ray Scattering Replication Data for: Radiolytic Degradation of Cellulosic Materials in Nuclear Waste: Effect of Oxygen and Absorbed Dose. KU Leuven Research Data Repository. <https://doi.org/10.48804/IPOIL9>.
- Fernandez, A., Ooms, H., Brichard, B., Coeck, M., Coenen, S., Berghmans, F., 2002. Test facilities at SCK CEN for radiation tolerance assessment: from space applications to fusion environments. In: *Proceedings of the RADECS 2002 Workshop*. Padua, Italy, pp. 200–204.
- Gaona, X., Montoya, V., Colas, E., Grive, M., Duro, L., 2008. Review of the complexation of tetravalent actinides by ISA and gluconate under alkaline to hyperalkaline conditions. *J. Contam. Hydrol.* 102, 217–227. <https://doi.org/10.1016/j.jconhyd.2008.09.017>.
- García, E., Johnston, D., Whitaker, J.R., Shoemaker, S.P., 1993. Assessment of endo-1,4-beta-D-glucanase activity by a rapid colorimetric assay using disodium 2,2'-bicinechinate. *J. Food Biochem.* 17, 135–145. <https://doi.org/10.1111/j.1745-4514.1993.tb00463.x>.
- Gentile, V.M., Schroeder, L.R., Atalla, R.H., 1987. Physical structure and alkaline degradation of hydrocellulose. In: Atalla, R.H. (Ed.), *The Structures of Cellulose*. American Chemical Society, pp. 272–291. <https://doi.org/10.1021/bk-1987-0340.ch016>.
- Glaus, M.A., Van Loon, L.R., Schwyn, B., Vines, S., Williams, S.J., Larsson, P., Puigdomenech, I., 2008. Long-term predictions of the concentration of alpha-isosaccharinic acid in cement pore water. In: Lee, W.E., Roberts, J.W., Hyatt, N.C., Grimes, R.W. (Eds.), *Scientific Basis for Nuclear Waste Management XXXI*. Materials Research Society, pp. 605–612. <https://doi.org/10.1557/PROC-1107-605>.
- Gomez, L.D., Steele-King, C.G., McQueen-Mason, S.J., 2008. Sustainable liquid biofuels from biomass: the writing's on the walls. *New Phytol.* 178, 473–485. <https://doi.org/10.1111/j.1469-8137.2008.02422.x>.
- Haas, D.W., Hrutford, B.F., Sarkanen, K.V., 1967. Kinetic study on the alkaline degradation of cotton hydrocellulose. *J. Appl. Polym. Sci.* 11, 587–600. <https://doi.org/10.1002/app.1967.070110408>.
- Hallac, B.B., Ragauskas, A.J., 2011. Analyzing cellulose degree of polymerization and its relevancy to cellulosic ethanol. *Biofuel. Bioprod. Biorefin.* 5, 215–225. <https://doi.org/10.1002/bbb.269>.
- Henniges, U., Okubayashi, S., Rosenau, T., Potthast, A., 2012. Irradiation of cellulosic pulps: understanding its impact on cellulose oxidation. *Biomacromolecules* 13, 4171–4178. <https://doi.org/10.1021/bm3014457>.
- Inagaki, T., Siesler, H.W., Mitsui, K., Tsuchikawa, S., 2010. Difference of the crystal structure of cellulose in wood after hydrothermal and aging degradation: a NIR Spectroscopy and XRD Study. *Biomacromolecules* 11, 2300–2305. <https://doi.org/10.1021/bm100403y>.
- Ioelovich, M.Y., 2016. Models of supramolecular structure and properties of cellulose. *Polym. Sci. Ser. A* 58, 925–943. <https://doi.org/10.1134/S0965545X16060109>.
- ISO, 2019. Paper, Board, Pulps and Cellulose Nanomaterials - Determination of Residue (Ash Content) on Ignition at 525 °C. ISO standard ISO 1762.
- ISO/ASTM, 2013. Practice for Dosimetry in Radiation Processing, 52628, p. 2013 (E).
- Khan, F., Ahmad, S.R., Kronfli, E., 2006. γ -Radiation induced changes in the physical and chemical properties of lignocellulose. *Biomacromolecules* 7, 2303–2309. <https://doi.org/10.1021/bm060168y>.
- Klemm, D., Philipp, B., Heinze, T., Wagenknecht, W., 1998. *Comprehensive Cellulose Chemistry*. In: *Fundamentals and Analytical Methods*, ume 1. Wiley-VCH Verlag GmbH.
- Kongruang, S., Han, M.J., Breton, C.I.G., Penner, M.H., 2004. Quantitative analysis of cellulose-reducing ends. *Appl. Biochem. Biotechnol.* 113, 213–231. <https://doi.org/10.1385/ABAB:113:1:3:213>.
- Kontturi, E., Tammelin, T., Österberg, M., 2006. Cellulose—model films and the fundamental approach. *Chem. Soc. Rev.* 35, 1287–1304. <https://doi.org/10.1039/B601872F>.
- Kovalev, G., Bugaenko, L., 2003. On the crosslinking of cellulose under exposure to radiation. *High Energy Chem.* 37, 209–215. <https://doi.org/10.1023/A:1024790415083>.
- Kulasinski, K., Keten, S., Churakov, S.V., Derome, D., Carmeliet, J., 2014. A comparative molecular dynamics study of crystalline, paracrystalline and amorphous states of cellulose. *Cellulose* 21, 1103–1116. <https://doi.org/10.1007/s10570-014-0213-7>.
- Kusama, Y., Kageyama, E., Shimada, M., Nakamura, Y., 1976. Molecular weights and molecular weight distributions of irradiated cellulose fibers by gel permeation chromatography. *J. Appl. Polym. Sci.* 20, 1679–1688. <https://doi.org/10.1002/app.1976.070200626>.
- LaVerne, J.A., Driscoll, M.S., Al-Sheikhly, M., 2020. Radiation stability of lignocellulosic material components. *Radiat. Phys. Chem.* 171, 108716. <https://doi.org/10.1016/j.radphyschem.2020.108716>.
- Martínez-Sanz, M., Pettolino, F., Flanagan, B., Gidley, M.J., Gilbert, E.P., 2017. Structure of cellulose microfibrils in mature cotton fibers. *Carbohydr. Polym.* 175, 450–463. <https://doi.org/10.1016/j.carbpol.2017.07.090>.
- Mittal, A., Katahira, R., Himmel, M.E., Johnson, D.K., 2011. Effects of alkaline or liquid-ammonia treatment on crystalline cellulose: changes in crystalline structure and effects on enzymatic digestibility. *Biotechnol. Biofuels* 4, 41. <https://doi.org/10.1186/1754-6834-4-41>.
- Moodley, P., Trois, C., 2021. 2 - lignocellulosic biorefineries: the path forward. In: Ray, R.C. (Ed.), *Sustainable Biofuels*. Academic Press, pp. 21–42. <https://doi.org/10.1016/B978-0-12-820297-5.00010-4>.
- Moon, R.J., Martini, A., Nairn, J., Simonsen, J., Youngblood, J., 2011. Cellulose nanomaterials review: structure, properties and nanocomposites. *Chem. Soc. Rev.* 40, 3941–3994. <https://doi.org/10.1039/c0cs00108b>.
- Nishiyama, Y., Kim, U.-J., Kim, D.-Y., Katsumata, K.S., May, R.P., Langan, P., 2003. Periodic disorder along ramie cellulose microfibrils. *Biomacromolecules* 4, 1013–1017. <https://doi.org/10.1021/bm025772x>.
- Nishiyama, Y., Langan, P., Chanzy, H., 2002. Crystal structure and hydrogen-bonding system in cellulose I β from synchrotron X-ray and neutron fiber diffraction. *J. Am. Chem. Soc.* 124, 9074–9082. <https://doi.org/10.1021/ja0257319>.
- Pitkänen, L., Sixta, H., 2020. Size-exclusion chromatography of cellulose: observations on the low-molar-mass fraction. *Cellulose* 27, 9217–9225. <https://doi.org/10.1007/s10570-020-03419-9>.
- Ponomarev, A., Ershov, B., 2014. Radiation-induced high-temperature conversion of cellulose. *Molecules* 19, 16877. <https://doi.org/10.3390/molecules191016877>.
- Ramírez-Cahero, H.F., Valdivia-López, M.A., 2018. Effect of gamma radiation on sugars and vitamin C: radiolytic pathways. *Food Chem.* 245, 1131–1140. <https://doi.org/10.1016/j.foodchem.2017.11.057>.
- Sánchez Orozco, R., Balderas Hernández, P., Flores Ramírez, N., Roa Morales, G., Saucedo Luna, J., Castro Montoya, A.J., 2012. Gamma irradiation induced degradation of orange peels. *Energies* 5, 3051–3063. <https://doi.org/10.3390/en5083051>.
- Sarosi, O.P., Bischof, R.H., Potthast, A., 2020. Tailoring pulp cellulose with electron beam irradiation: effects of lignin and hemicellulose. *ACS Sustain. Chem. Eng.* 8, 7235–7243. <https://doi.org/10.1021/acssuschemeng.0c02165>.
- TAPPI, 2009. Alpha-, Beta- and Gamma-Cellulose in Pulp. TAPPI standard T 203 cm-09.
- TAPPI, 2021. Acid-insoluble Lignin in Wood and Pulp. TAPPI standard T 222 om-21.
- Udegraff, D.M., 1969. Semimicro determination of cellulose in biological materials. *Anal. Biochem.* 32, 420–424. [https://doi.org/10.1016/S0003-2697\(69\)80009-6](https://doi.org/10.1016/S0003-2697(69)80009-6).
- Van Loon, L.R., Glaus, M.A., 1997. Review of the kinetics of alkaline degradation of cellulose in view of its relevance for safety assessment of radioactive waste repositories. *J. Environ. Polym. Degrad.* 5, 97–109. <https://doi.org/10.1007/BF02763593>.
- Van Loon, L.R., Glaus, M.A., 1998. Experimental and theoretical studies on alkaline degradation of cellulose and its impact on the sorption of radionuclides, 07 PSI-Bericht 98. PSI, Villigen, Switzerland.
- Van Loon, L.R., Glaus, M.A., Laube, A., Stallone, S., 1999. Degradation of cellulosic materials under the alkaline conditions of a cementitious repository for low- and intermediate level radioactive waste. Part III: effect of degradation products on the sorption of radionuclides on feldspar. *Radiochim. Acta* 86, 183–189. <https://doi.org/10.1524/ract.1999.86.34.183>.
- Vercammen, K., Glaus, M.A., Van Loon, L.R., 1999. Evidence for the existence of complexes between Th(IV) and alpha-isosaccharinic acid under alkaline conditions. *Radiochim. Acta* 84, 221–224. <https://doi.org/10.1524/ract.1999.84.4.221>.
- Von Sonntag, C., Dizdaroglu, M., Schulte-Frohlinde, D., 1976. Radiation chemistry of carbohydrates. VIII. γ -Radiolysis of cellobiose in N₂O-saturated aqueous solution. Part II. Quantitative measurements. Mechanisms of the radical-induced scission of the glycosidic linkage. *Z. Naturforsch. B Chem. Sci.* 31, 857–864. <https://doi.org/10.1515/znb-1976-0627>.
- Vonk, C.G., 1973. Computerization of Ruland's X-ray method for determination of the crystallinity in polymers. *J. Appl. Crystallogr.* 6, 148–152. <https://doi.org/10.1107/S0021889873008332>.